Metrology Sensor Characterization and Pointing Control for the Formation Interferometer Testbed (FIT)

Joel Shields, Sam Sirlin, Matt Wette
Jet Propulsion Laboratory
4800 Oak Grove Drive
Pasadena CA 91109-8099
818-354-5050
Joel.F.Shields@jpl.nasa.gov

Abstract— StarLight is a NASA\JPL sponsored mission that will demonstrate formation flying and interferometric technologies needed for future missions such as Terrestrial Planet Finder (TPF). The StarLight stellar interferometer is composed of two spacecraft, a combiner spacecraft and a collector spacecraft, forming separated apertures.

In this paper, the metrology pointing sensor of the StarLight ground instrument prototype is characterized and a siderostat pointing control loop is closed between two optical benches with a 10 meter separation. The Formation Interferometer Testbed (FIT) metrology pointing sensor (MPS) uses four photodiodes to detect gradients in the metrology laser caused by relative motion of the two optical benches. By differencing across the photodiodes, a measurement of the laser beam centroid can be obtained. In the flight design, this signal is passed to the combiner spacecraft, via an interspacecraft communication link, and used as a feedback signal to point a siderostat on the combiner spacecraft.

In this paper, a detailed model of the metrology pointing sensor is described based exclusively on experimental data. Both the sensitivity and dynamic range of the sensor are effectively described by this model. The effect of diffraction in the laser light and air path noise on the sensor performance are evaluated.

A nonlinear estimation algorithm is proposed that is capable of increasing the capture zone of the sensor by a factor of two. This algorithm relies on using the photodiode sum as an additional measurement.

The second part of this paper describes a siderostat pointing control algorithm that uses tachometer, encoder, and the metrology pointing sensor as feedback signals in a nested loop architecture. Experimental results are included that demonstrate the tracking ability of this controller in the presence of spacecraft relative motion caused by Attitude Control System (ACS) deadbands.

TABLE OF CONTENTS

0-7803-7231-X/01/ 10.00 ©2002 IEEE

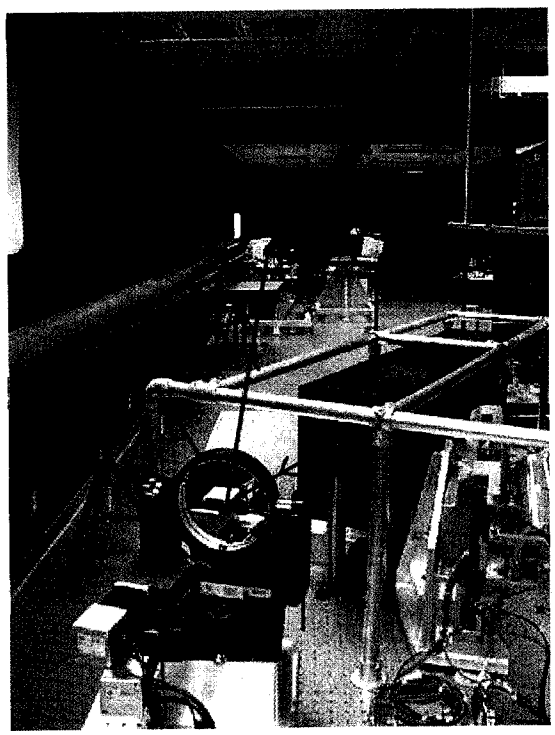

Figure 1. Photograph of the left side of the FIT instrument. The path of the interspacecraft metrology beam is denoted with annotated lines. In the foreground is the left siderostat. The metrology pointing sensor (IGD) is in the background mounted on the collector bench.

1. INTRODUCTION

The FIT interferometer is a ground based prototype of the two spacecraft StarLight instrument. StarLight is a NASA/JPL sponsored technology development mission that will demonstrate formation flying of two spacecraft and interferometric stellar observations [1]. Both spacecraft are used to collect light from separated apertures which is then combined to produced interference fringes

on the combiner spacecraft. The interspacecraft metrology pointing system is used to maintain an optical link between the two spacecraft and thereby keep the boresights of the metrology and starlight co-aligned. Maintaining the metrology lock is also necessary to ensure a return signal for the interspacecraft metrology gauge that is used to estimate the fringe position. Furthermore, information from the metrology pointing system, in the form of range and bearing measurements, can be used by the formation estimator to calibrate the autonomous formation flying (AFF) sensors.

The pointing system is composed of a large aperture siderostat on the left side of the combiner spacecraft and a pointing sensor on the collector spacecraft. The pointing sensor is a JPL design developed specifically for the StarLight mission [2]. It is an array of four photodiodes (See Figure 2.) that are selectively sensitive to the wavelength of the metrology laser. By differencing across the photodiodes, measurements of the laser beam position can be derived which are then transferred across a communication link to the combiner spacecraft and used as feedback signals to point the left combiner siderostat.

The metrology pointing sensor assumes that the metrology beam has a Gaussian distribution of intensity and operates by detecting gradients in the photodiode voltages caused by translation of the beam across the face of the sensor. The measurement equations for the sensor are,

$$V_{nx'} = \frac{(V_{igd3} + V_{igd1}) - (V_{igd4} + V_{igd2})}{(V_{igd1} + V_{igd2} + V_{igd3} + V_{igd4} + V_{bias})} \quad (1)$$

$$V_{ny'} = \frac{(V_{igd4} + V_{igd3}) - (V_{igd2} + V_{igd1})}{(V_{igd1} + V_{igd2} + V_{igd3} + V_{igd4} + V_{bias})} \quad (2)$$

where $V_{(\cdot)}$ are the photodiode voltages and V_{bias} is a constant ($V_{bias} = -1$) that is used to keep the measurements well defined when the beam is far from the sensor. Note that $V_{nx'}$ is a measurement of the beam location in the x' direction and $V_{ny'}$ is a measurement of the beam location in the y' direction (Refer to Figure 2 for coordinate frame definitions.).

The FIT testbed is comprised of three main optical benches. The main bench is the combiner bench which collects light on the right side of the instrument from the pseudostar bench and on the left side of the instrument from the collector bench. The collector bench is mounted on a 6 DOF hexapod which allows simulation of spacecraft relative motion, caused in flight, by thruster ACS deadbands. A photo of the left side of the instrument is shown in Figure 1. Note the tube to the left of the photo that can be installed along the path of the metrology beam to reduce the effect of air turbulence.

The siderostat (Aerotech, AOM130-6M) used for metrology pointing has local feedback of both position and velocity provided by encoders mounted on the shafts of two DC motors (BM75E). The amplifiers (BAL 20-40-A) were configured in velocity mode to reduce the effect of friction. The position loop has a closed loop bandwidth of approximately 40 Hertz in both azimuth and elevation axes.

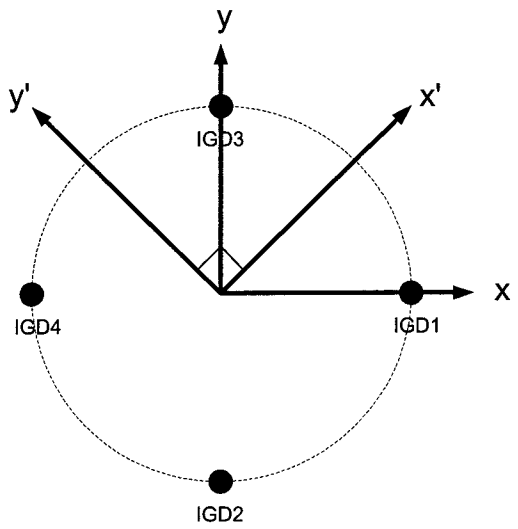

Figure 2. Intensity gradient detector (IGD) photodiode arrangement and coordinate frames. The primed frame is referred to as the sensor frame and the unprimed frame is referred to as the vertical frame.

2. System Characterization

Backlash Investigation

The fundamental limitation on the pointing accuracy of the Aerotech siderostats is backlash in the drive mechanism. The Aerotech siderostats are equipped with a 1000 line encoder which, with 4X quadrature and a gear ratio of 25816.7:1, provide a knowledge resolution of up to 12.5 milli-arc seconds at the gimbals. This accuracy cannot be achieved, however, because of backlash in the gimbal drive mechanism.

To determine the actual pointing accuracy, the gimbal position was directly measured using laser metrology. A silicon based light sensitive position sensing device (OnTrak PSM with OT-301 amplifier) with a calibrated scale factor of 2.0e-4 m/volt was used in conjunction with a He-Ne laser source reflected off the mirror to measure the true position of the siderostat gimbal. The PSM was placed 1.16 meters from the mirror with the reflected laser beam impacting the silicon die. An open loop velocity command (either sine or triangle wave) was applied to a given axis while data was recorded from both the encoder and PSM. Results for the azimuth axis are shown in Figure 3. The backlash is clearly detected as the separation of the two lines in this figure. At the azimuth encoder the backlash is approximately 0.175 radians. This represents 1.4 arc seconds of backlash at the

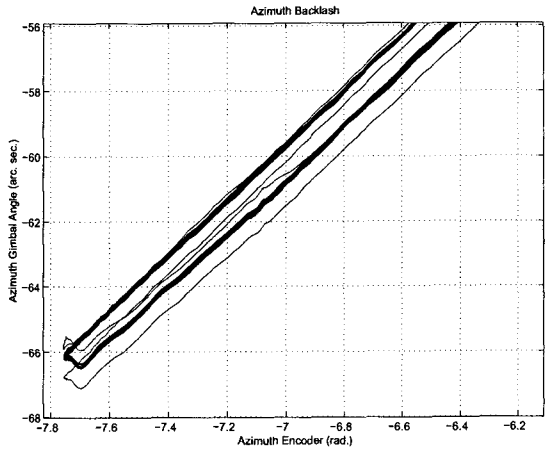

Figure 3. Backlash of the siderostat azimuth axis. Measurements from both the azimuth encoder (x-axis) and angular metrology (y-axis) were used to discern the effect of backlash.

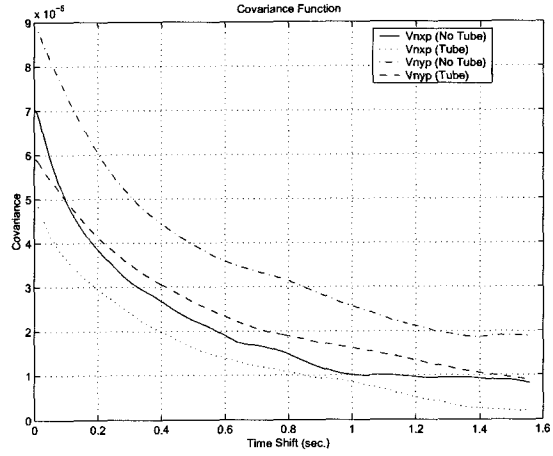

Figure 4. Auto-covariance function of sampled IGD signals with and without a tube installed along the exposed air path.

azimuth gimbal, much greater than the encoder resolution would predict. The elevation axis was found to have about 0.39 arc seconds of backlash at the gimbal. In both cases the amount of backlash was found to be highly dependent on position.

As to the exact source of the backlash, some simple calculations reveal that the likely culprit is a threaded rod in the Aerotech mounts. The Aerotech drive mechanism is a three stage device. The first stage consists of two sets of spur gears each with a gear ratio of 5:1, for an effective gear ratio, GR_{spur}, of 25:1. The output shaft of the gear box drives a threaded rod with a pitch, p, of 0.113 mm/radian. A universal joint then connects a nut driven by the threaded rod to a lever arm, r, of length 0.115 meters which acts to move the gimbal axis. The overall gear ratio of the three stages is,

$$GR = GR_{spur} \cdot \frac{1}{p} \cdot r. \tag{3}$$

The first spur gear has 20 teeth which means that for the azimuth axis, there would have to be 0.5 teeth of backlash at this point to explain the amount of backlash seen in this axis. The second contact point in the spur gear box would require 0.1 teeth of backlash. In either case, it is unlikely that there is this much backlash in the gear box, so the source of the backlash is likely after the gear box. The amount of play at the threaded rod to explain 1.4 arc seconds of backlash at the gimbal is only 0.78 microns, or one 886.1th of a thread. This is much more likely the source of the backlash. If the backlash is at this level, preloading the gimbal should help reduce the backlash which was, in fact, found to be the case.

Air Path Disturbance Modelling

In the FIT laboratory the metrology beam is deflected from its nominal path by air currents in the lab. On the left side of the interferometer, this error is sensed at the transfer flat on the collector bench by the IGD sensor, and can be rejected by moving the left combiner siderostat in an appropriate manner. In flight, this feedback loop acts to take out any attitude and translational deadbands caused by the spacecraft ACS. In the FIT lab these deadbands are simulated by moving the collector hexapod. Thus, in the laboratory, the IGD loop has the duel job of taking out the relatively low frequency interspacecraft motion and, if possible, reject the pointing error caused by the higher frequency air path disturbance.

The air path disturbance is by its nature stochastic, but observations of the photodiode voltages (sampled at 256 Hz) reveal that it is correlated in time. Figure 4 reveals that the air path process has a correlation time of approximately 0.3 seconds. This figure is a plot of the auto-covariance function,

$$X_{xx}(\tau) = E\left[(x(\tau) - m_x)(x(t-\tau) - m_x)\right], \tag{4}$$

where $E[\cdot]$ is the expectation operator, and m_x is the mean value of the signal $x(t)$, for the normalized IGD measureables, $V_{nx'}$ and $V_{ny'}$, with and without the tube installed between the optical benches. Note that with the tube, the variance at all time shifts, τ, is smaller than without the tube. Thus, the tube is somewhat effective at reducing the effect of air turbulence on the beam path. This is what one would expect since the volume of air that the metrology beam passes through is contained and isolated from the external environment when the tube is present. The square root of the peak value of the curves in Figure 4 represents the standard deviation of the air path disturbance. The noise equivalent angle (NEA) at the siderostat gimbal due to the

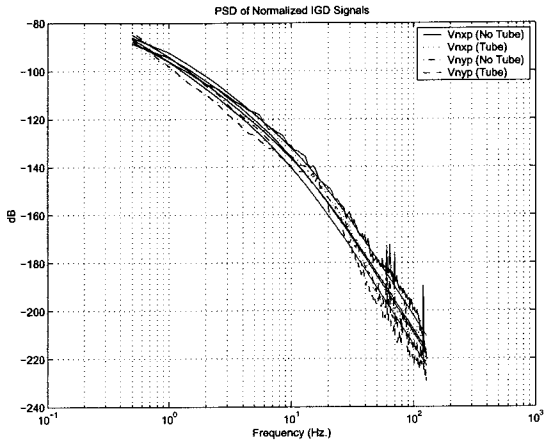

Figure 5. PSD of normalized IGD signals with and without a protective tube installed to mitigate the air path turbulence. Solid lines represent a parametric fit of the frequency domain data.

effect of air path is,

$$NEA_{V_{nx'}} = \frac{2\sigma_{V_{nx'}} SG^{-1}_{V_{nx'}}}{2R} = \pm 1.056 \ (arc\,seconds),$$
$$NEA_{V_{ny'}} = \frac{2\sigma_{V_{ny'}} SG^{-1}_{V_{ny'}}}{2R} = \pm 1.159 \ (arc\,seconds) \tag{5}$$

where R (10.26 meters) is the distance between the left combiner siderostat and the collector IGD sensor and $SG_{(\cdot)}$ is the scale factor between $V_{n(\cdot)}$ and the displacement of the beam centroid in the IGD coordinate frame. $SG_{V_{nx'}}$ and $SG_{V_{ny'}}$ were calculated by commanding the left combiner siderostat in azimuth and elevation a known amount, and recording the resulting $V_{nx'}$ and $V_{ny'}$ values. A linear fit to this data gave $SG_{V_{nx'}} = 160.86$ 1/meters and $SG_{V_{ny'}} = 163.64$ 1/meters.

For the FIT interferometer ~ 1.0 arc seconds of beam jitter at the left siderostat gimbal represents about 50 microns of shear between the metrology and stellar beams at the IGD transfer flat. This small amount of shear is not be large enough to cause any alignment problems in the combiner optics with either the incoming stellar light or return metrology signal.

In order to simulate the effect of the air path turbulence on the pointing control loops, a shaping filter can be designed to match the spectral content of the air path disturbance. The PSD of the sampled time series for $V_{nx'}(t)$ and $V_{ny'}(t)$ is shown in Figure 5. The slope in this plot is -80 dB/decade which indicates that a second order transfer function is needed to model the spectral content of the sampled data. Assuming a two pole model of the form,

$$H(s) = \frac{k}{s^2 + as + b}, \tag{6}$$

where we take as the input, zero mean Gaussian white noise, $w(t)$, with auto-covariance function,

$$E\left[w(t)w(t-\tau)\right] = Q\delta(\tau), \quad (Q = 1) \tag{7}$$

we can parameterize $|H(j\omega)|^2$ in the following linear form,

$$\underbrace{\psi(\omega)\omega^4}_{\mathbf{Y}} = \underbrace{\left[-\psi(\omega)\omega^2 \quad -\psi(\omega) \quad 1\right]}_{\mathbf{A}} \underbrace{\begin{bmatrix} a^2 - 2b \\ b^2 \\ k^2 \end{bmatrix}}_{\mathbf{\Theta}}, \tag{8}$$

where $\psi(\omega)$ is the spectral power, $|H(j\omega)|^2$, at a given frequency, ω. To solve for the transfer function parameters, $\mathbf{\Theta}$, this equation can be inverted using a frequency weighted least squares calculation,

$$\mathbf{\Theta} = (\mathbf{A^T W A})^{-1}\mathbf{A^T W Y}, \tag{9}$$

where $\mathbf{W}$ is the weighting matrix (diagonal), $\mathbf{Y} \in \Re^{\mathbf{n\times 1}}$ is the vector of left hand values of Equation (8) at n frequency points, and $\mathbf{A} \in \Re^{\mathbf{n\times 3}}$ is the matrix of regressor vectors. This calculation results in the following shaping filters for the case of no tube in the beam path.

$$V_{nx'}(s) = \frac{3.5}{s^2 + 98.1s + 409.1} w_{V_{nx'}}(s)$$
$$V_{ny'}(s) = \frac{2.5}{s^2 + 85.8s + 211.6} w_{V_{nx'}}(s) \tag{10}$$

For implementation in the pointing simulation testbed, these filters were converted to a state space realization and discretized using a first order approximation of the state transition matrix.

$$\dot{\mathbf{x}}(t) = \mathbf{A}\mathbf{x}(t) + \mathbf{B}w(t), \quad V = \mathbf{C}\mathbf{x}(t) \quad \Rightarrow$$
$$\mathbf{x}((k+1)\Delta t) = \mathbf{A}_d\mathbf{x}(k\Delta t) + \mathbf{B}_d\mathbf{w}_d(k\Delta t),$$
$$V_{n(\cdot)}(k\Delta t) = \mathbf{C}\mathbf{x}(k\Delta t) \tag{11}$$

The matrices $\mathbf{A}_d$ and $\mathbf{B}_d$ are defined based on the solution of the continuous time system at discrete time intervals.

$$\mathbf{A}_d = \exp(\mathbf{A}\Delta t) \tag{12}$$
$$\mathbf{B}_d\mathbf{B}_d^T = \mathbf{\Gamma} \tag{13}$$
$$\mathbf{\Gamma} = \exp(\mathbf{A}\Delta t)[\mathbf{B}Q\mathbf{B}^T\Delta t - \frac{1}{2}\Delta t^2\mathbf{B}Q\mathbf{B}^T\mathbf{A}^T$$
$$-\frac{1}{2}\Delta t^2\mathbf{A}\mathbf{B}Q\mathbf{B}^T + \frac{1}{3}\Delta t^3\mathbf{A}\mathbf{B}Q\mathbf{B}^T\mathbf{A}^T](\exp(\mathbf{A}\Delta t))^T \tag{14}$$

The factorization of $\mathbf{B}_d$ in Equation (13) is performed using a Cholesky decomposition. Note that even though the continuous time system has a scalar random input, the equivalent discrete time system has a vector random input with auto-covariance function,

$$E\left[\mathbf{w}_d(k)\mathbf{w}_d(j)\right] = \mathbf{\Gamma}\delta_{kj}. \tag{15}$$

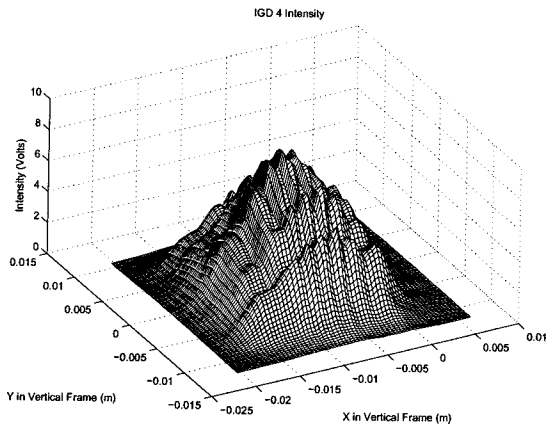

Figure 6. Output voltage of the 4th photodiode as a function of metrology beam location. Note diffraction ripples in both directions caused by the square aperture of the metrology spider.

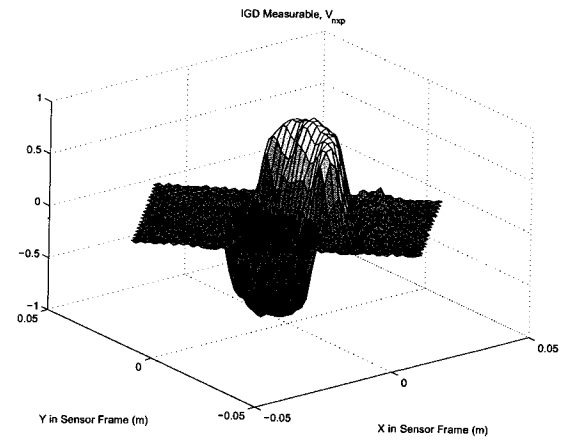

Figure 7. Plot of $V_{nx'}$ as a function of beam position. Note irregularities in the surface along the cross axis.

In characterizing the air path disturbance we have assumed that the random variations in the sampled IGD voltages are due to air currents and not vibrations of the optical bench. If vibrations were responsible for the variations observed from the IGD signals, one would expect that the 4 IGD voltages would be highly correlated in time with one another. This was found not to be the case, however, as the largest correlation coefficient was found to be 0.56, which means only $\sim$ 25 percent of the data in a scatter (x-y) plot between any two of the IGD voltages can be explained using a linear relationship . In either case, the source of the variations are of secondary interest as the control loops will act to reject these disturbances regardless of their source.

Another finding on the effect of air path turbulence in the FIT laboratory is that the amount of pointing error caused by the air path disturbances does not depend on distance. This is perhaps counter to what one might initially think. This effect was observed during the backlash investigation by placing the PSM at different distances from the siderostat mirror. The motivation for doing this was to see which placement gave the best resolution of gimbal angle. For the three distances, 210 mm, 1700 mm, and 10000 mm that were tried, the amplitude of the air path disturbance calculated by,

$$Beam\ Error = \frac{V_{p-p} \cdot 0.2\,(mm/volt)}{range}, \qquad (16)$$

where V_{p-p} is the quiescent (i.e. no siderostat motion) peak to peak variation in PSM voltage, was found to be approximately 1.0 arc seconds for all three placements of the sensor. This implies that the air turbulence causes V_{p-p} to scale linearly with range.

Sensor Characterization

The previous section characterized the stochastic behavior of the IGD signals. What remains, is to determine the bias in each of the IGD signals as a function of the beam displacement. We already have a coarse model for the bias from calculating $SG_{V_{nx'}}$ and $SG_{V_{ny'}}$ in Equations (5). A more accurate model of the static IGD output was obtained by scanning the metrology beam across the face of the transfer flat and sampling the four IGD signals. The scanning was sinusoidal in the azimuth direction and ramped downward in the elevation direction from a position slightly above the IGD sensor. Figure 6 shows the result of this experiment for the 4th IGD photodiode. This figure is essentially a photograph of the metrology beam intensity. To model the IGD sensor in the simulation testbed, look up tables containing the data shown in Figure 6, for each of the four photodiodes were used.

Note the diffraction pattern that is superimposed on Figure 6. This pattern is caused by obscuration of the metrology beam as it exits the square aperture of a metrology spider located on the combiner bench. The effect of these ripples, together with possibly too large of a photodiode radius relative to the beam diameter, is to introduce a large amount of uncertainty in the relationship between the IGD measurables, Equations (1)-(2), and beam location. Knowledge of this relationship becomes important during design of the metrology pointing control algorithm. In addition, if an estimator (i.e. Kalman Filter) is used to estimate the impact position of the metrology beam based on IGD measurements, this uncertainty could cause either local minimum in the optimization algorithm or large estimation errors due to the modelling error introduced by the smoothing of the surfaces that would be necessary. These effects were observed using an estimator design based on Fourier transforms to model the surface functions $V_{nx'} = V_{nx'}(x', y')$ and $V_{ny'} = V_{ny'}(x', y')$.

what?

Figure 7 is a plot of $V_{nx'}(x', y')$. Note in this figure that the IGD measurable, $V_{nx'}$, is not a single valued function. The measurement is linear within a certain distance ($\sim \pm 6.0$ mm) of the photodiode array center, beyond which it de-

creases back to zero as the beam no longer exposes any of the photodiodes. As a result, the capture range of the sensor is restricted to be within the linear range, since otherwise it would not be possible to discern, from a given measurement, whether or not the beam was inside or outside of the linear range. To overcome this limitation, measurements (1) and (2) can be augmented with the sum measureable,

$$V_\Sigma = V_{igd1} + V_{igd2} + V_{igd3} + V_{igd4}. \qquad (17)$$

The sum information is enough to clarify the beam position ambiguity. If the sum is large, then the beam is within the linear region, else if the sum is small then the beam is outside the linear region. An estimator of the beam position would then use measurements in the form of,

$$\begin{bmatrix} V_{nx'} \\ V_{ny'} \\ V_\Sigma \end{bmatrix} = \mathbf{h}(x', y'), \qquad (18)$$

where $\mathbf{h}(x', y')$ is a highly nonlinear vector function. Theoretically, with noiseless measurements, this approach offers the possibility of making the capture range of the sensor infinite. Practically, however, we should expect a 2X increase in the capture range. This idea is not pursued further in this paper as it would require a significant divergence from the intended topics of the paper.

3. Acquisition

The acquisition of the metrology signal is a critical step in the observation sequence of the instrument. It represents the first optical link between the two spacecraft and is a prerequisite for acquisition of the left side starlight. To acquire feedback signals from the IGD sensor for the metrology loop, a spiral search is performed. The search is designed to be optimal within the constraint that the velocity limits on the siderostat are never exceeded. To achieve this, we parameterize the search in polar coordinates with,

$$\begin{aligned} r &= \frac{g}{2\pi}\theta \\ \theta &= f(t), \end{aligned} \qquad (19)$$

where r and θ are the polar coordinates of a cartesian frame located at the center of the IGD sensor. g is the spacing between adjacent spirals, which should be configured to be less then the dynamic range of the IGD sensor. $f(t)$ is some, as yet, undetermined function of time. This function can be specified by observing that if the local velocity along the pathlength of the spiral is constant, the velocity commands to the siderostat axes will be sinusoids with a constant amplitude. This amplitude can be adjusted to be slightly less than the siderostat velocity limit by specifying the pathlength velocity. In cartesian coordinates the pathlength velocity is given by,

$$s = \sqrt{\dot{x}^2 + \dot{y}^2}, \qquad (20)$$

where,

$$\begin{aligned} x &= r\cos(\theta) \\ y &= r\sin(\theta). \end{aligned} \qquad (21)$$

Substituting Equations (21) and (19) into (20), we arrive at the following differential equation,

$$\dot{f}(t) = \pm\sqrt{\frac{(2\pi s/g)^2}{1 + f(t)^2}} \qquad f(0) = 0, \qquad (22)$$

which describes the time evolution of $\theta(t)$ for the optimal spiral search. This equation was solved numerically, in real time, for trajectory generation of the acquisition spiral. The $(+)$ solution is used for outward spirals and the $(-)$ solution is used for inward spirals. The siderostat encoder commands are obtained from,

$$\begin{aligned} \theta_{El.} &= -\left(\frac{y}{2d}\right) \cdot GR \\ \theta_{Azi.} &= -\left(\frac{x}{2d}\right) \cdot GR, \end{aligned} \qquad (23)$$

where x and y come from Equation (21) and d is the separation between the spacecraft.

Although we have formulated the problem with respect to constraints on the siderostat velocity, the solution is also applicable to situations which have a velocity constraint on the spiral imposed by the sensor's ability to detect changing signals.

4. Controller Design

A model of the pointing system is shown in Figure 8. This model includes three effects on the beam position sensed by the IGD sensor. First, is the effect from moving the siderostats, which is the controlled variable in the system. Second, is the stochastic air path disturbance. Third is the hexapod motion which is modelled as a ramp position disturbance. Even though the actual interaction of the 6 DOF hexapod motion with the IGD sensor is much more complicated, this model should be adequate for the small translations and rotations of the hexapod that simulate thruster deadbands.

Note that because the siderostat azimuth and elevation axes control the beam position in vertical frame, and the measurements are made in the sensor frame, the sensor and actuator are coupled by the rotation matrix, $\mathbf{R}_z^T$. The matrix $\mathbf{K}$ in Figure 8 represents the interspacecraft kinematics, which for the flight system would include the effects of spacecraft attitudes and relative position. For the FIT lab, this matrix was taken to be simply,

$$\mathbf{K} = \begin{bmatrix} -2 \cdot R & 0 \\ 0 & -2 \cdot R \end{bmatrix}. \qquad (24)$$

Looking a Figure 8, the controller first acts to invert the input\output relationship of the IGD sensor using a linear approximation,

$$SG^{-1} = \begin{bmatrix} SG_{V_{nx'}} & 0 \\ 0 & SG_{V_{ny'}} \end{bmatrix}^{-1}. \qquad (25)$$

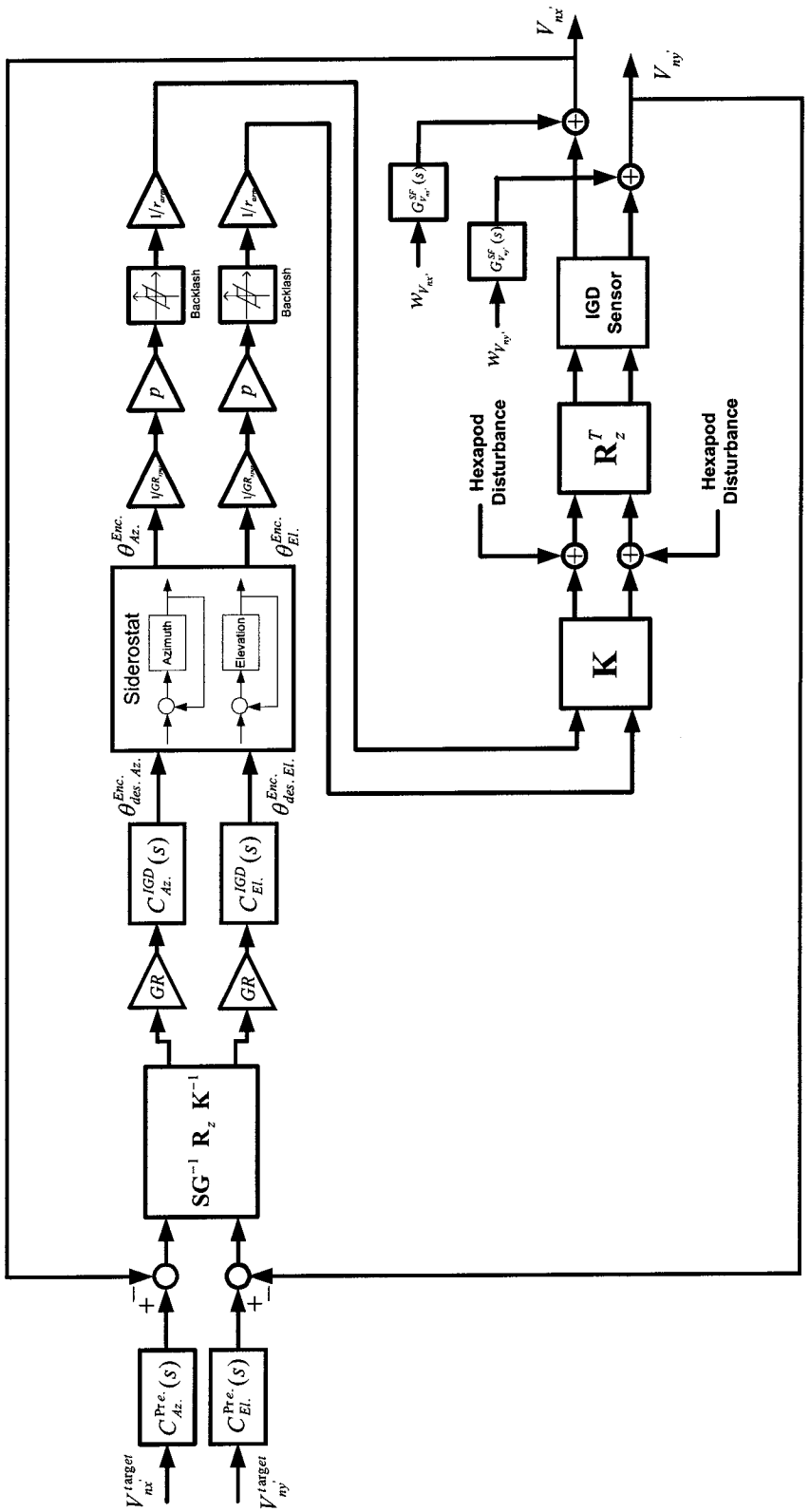

Figure 8. Model of IGD pointing system and control algorithm. The effect of hexapod motion, air path turbulence, and backlash are included in the pointing model. The controller diagonalizes the system and controls each axis as though they were SISO loops.

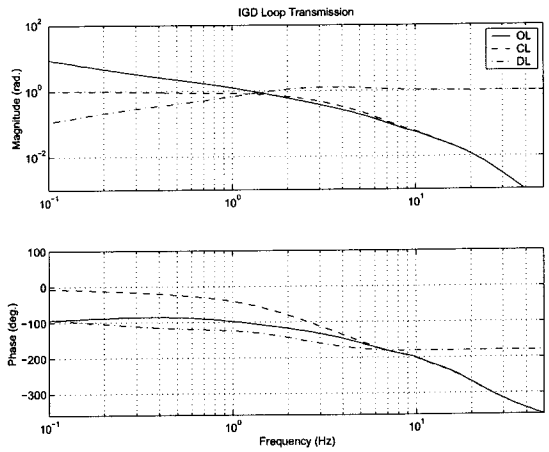

Figure 9. Open loop, closed loop, and disturbance attenuation of the metrology pointing system.

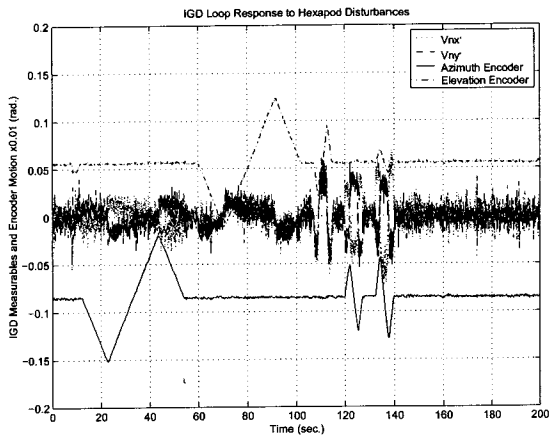

Figure 10. Experimental response of the metrology pointing system to disturbances introduced by hexapod motion.

The pointing system is then diagonalized by inverting the coupling between the sensor frame and siderostat gimbals. The error signal is then mapped to encoder space with the $\mathbf{K}^{-1}$ and GR control gains. With the system decoupled the dynamic part of the compensator can now be designed as if there were no coupling [3]. This is advantageous since SISO (Single Input Single Output) design can be less conservative then MIMO (Multiple Input Multiple Output) design. The azimuth and elevation loop shapes can be designed separately by treating,

$$C_{Az}^{IGD}(s)G_{Az}^{SD}(s) \tag{26}$$

$$C_{El}^{IGD}(s)G_{El}^{SD}(s) \tag{27}$$

as the effective open loop transfer functions. $G_{Az}^{SD}(s)$ and $G_{El}^{SD}(s)$ in these equations are the closed loop transfer functions from desired encoder position to actual encoder position.

Loop Shaping

To reject the air path disturbance the open loop control system must have a crossover well above the poles of the disturbance process. This ensures that the sensitivity of the control error to air path disturbances,

$$S(s) = \frac{-1}{1 + C_{(\cdot)}^{IGD}(s)G_{(\cdot)}^{SD}(s)}, \tag{28}$$

is small at frequencies where the disturbance is large. To achieve significant disturbance attenuation the compensator would have to be designed to provided an open loop bandwidth of approximately 50.0 Hz. Simulations of a system with this bandwidth displayed oscillatory behavior. The likely source of the instability was phase lag induced by the siderostat backlash [4]. It was empirically determined that the maximum bandwidth achievable in the laboratory was approximately 2.0 Hz (See Figure 9.). With this bandwidth, achieving any significant atmospheric rejection was not possible and the goal of the IGD control loop was limited to taking out the lower frequency hexapod motions.

Spacecraft thruster deadbands introduce "ramp" type disturbances into the metrology pointing system. In order to have zero steady state error with this type of disturbance, the compensator is required to have two integrators. Two phase lead components and a notch filter were added to achieve a graceful degradation of the phase in the crossover region. The overall compensator was 6th order. A prefilter was added to the input channels to avoid saturation from step changes in the target IGD measurables. Note that commands are given to the pointing loop in terms of desired $V_{nx'}$ and $V_{ny'}$ values. This is convenient in that commands between ± 1.0 are guaranteed to be within the capture range of the sensor.

Experimental Results

The response of the control system is shown in Figure 10. The hexapod was commanded to move in both translation and rotation. The translational motion was in a plane perpendicular to the metrology beam, first in the horizontal direction and second in the vertical direction, both at a rate of 0.5 mm/second., twice the "observation" mode control requirement for a 40 meter baseline [5]. The rotational motion was along each of the axes of the hexapod coordinate frame by an amount of ± 0.5 degrees.

Note that as the hexapod is slewed in the horizontal direction, the siderostat azimuth axis moves to track the location of the IGD. When the hexapod is slewed in the vertical direction, the elevation axis responds to track the IGD. In either case, the IGD signals asymptotically approach zero confirming proper operation of the control system. The second half of Figure 10 shows the response of the control system to rotational motion of the hexapod. The control errors are larger in this case, but the rotation rate was well above the attitude rate control specification [5].

5. Conclusions

This paper has presented a pointing model and control algorithm for the FIT angular metrology system. Performance of the system was demonstrated to be sufficient to cancel the effects of the spacecraft relative motion. For flight, it is anticipated that the basic structure of the algorithm could remain relatively unchanged. Modifications for varying baselines and changing relative attitudes of the two spacecraft should be straightforward. Since the IGD measurements are normalized, the sensor gain should be insensitive to attenuation of the beam intensity for larger spacecraft separations. In flight, a single calibration of the sensor at an intermediate spacecraft separation should be adequate for control purposes.

The backlash in the Aerotech siderostats was found to limit both the pointing accuracy and bandwidth of the control system. It should be mentioned that similar backlash numbers for this Aerotech model have been reported from the Keck interferometer. A direct drive gimbal would be more appropriate for interferometry applications.

References

[1] R. Duren and O. Lay, "The StarLight formation-flying interferometer system architecture," Big Sky, Montana, March 2002, IEEE Aerospace Conference, IEEE.

[2] A. Abramovici, "Intensity gradient detector for FIT: A user's guide," Tech. Rep., Jet Propulsion Laboratory, 2000.

[3] B. J. Lurie and P. J. Enright, *Classical Feedback Control With MATLAB*, Marcel Dekker Inc., New York, 2000.

[4] J. J. E. Slotine and W. Li, *Applied Nonlinear Control*, Prentice-Hall, 1991.

[5] A. Ahmed, "Starlight FACS requirements," 2001.

[6] M. Born and E. Wolf, *Principles of Optics*, Cambridge University Press, 1999.

[7] B. J. Lurie, J. J. Hench, A. Ahmed, and F. Y. Hadaegh, "Nonlinear control of the optical delay line pathlength," Orlando, Florida, April 1999, SPIE, vol. 3692, pp. 139–149.

[8] J. Shields, S. Sirlin, and M. Wette, "Starlight pointing subsystem for the formation interferometer testbed (FIT)," Big Sky, Montana, March 2002, IEEE Aerospace Conference, IEEE.

[9] R. K. Tyson, *Principles of Adaptive Optics*, Academic Press, 1991.

[10] J. W. Goodman, *Introduction to Fourier Optics*, McGraw-Hill, 1968.

[11] S. Dubovitsky, O. Lay, and A. Abramovici, "The StarLight metrology subsystem," Big Sky, Montana, March 2002, IEEE Aerospace Conference, IEEE.

Joel Shields *is a member of the Guidance and Control Analysis Group at the Jet Propulsion Laboratory. He received his B.S. degree in Applied Mechanics from U.C. San Diego in 1990 and his M.S. and Ph.D. degree in Control Systems from U.C. Berkeley in 1993 and 1997, respectively. His dissertation research was on control of exercise machines. He developed three exercise machine prototypes that use feedback from the user to actively change the workout based on a given performance criteria. He is the holder of a patent based on this work. Upon graduation, Dr. Shields worked as a consultant before joining the technical staff at JPL. Dr. Shields has extensive experience in design of mechatronic systems, system identification, adaptive control, precision servo control, and real time applications of control systems. Currently, he is working on pointing control for space based interferometry.*

Samuel Sirlin *has a Ph.D. in Mechanical Engineering from Columbia University (1983). From October 1983 to the present he has been a Member of the Technical Staff of JPL. His background and expertise covers the areas of dynamics and simulation, controls and estimation. During his time at JPL he has worked on a number of research and flight projects including Galileo, precision pointing, Ulysses, Control Structure Interaction research, Mars Pathfinder (launch vehicle stability analysis, attitude control design, landing system), inflatable antenna analysis and control, Modelling and Analysis for Controlled Optical Systems (MACOS), Integrated Modelling of Optical Systems (IMOS), Deep Space 1 (DS1), the DS1 rescue, Starlight, and Mars Exploratory Rover (MER). He has published 26 conference papers and 4 journal articles.*

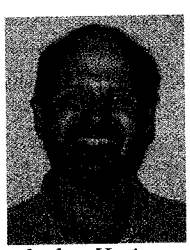

Matt Wette *is a Senior Engineer at the Jet Propulsion Laboratory in the Guidance and Control Analysis Group. His interests are in control system design, real-time systems, and discrete event control. Dr. Wette has contributed to several projects in the development of real-time simulation testbeds. He is currently working on interferometer control for the StarLight project.*

Metrology Sensor Characterization and Pointing Control for the Formation Interferometer Testbed (FIT)

Joel Shields, Sam Sirlin, Matt Wette
California Institute of Technology
Jet Propulsion Laboratory
4800 Oak Grove Drive
Pasadena CA 91109-8099
818-354-5050
Joel.F.Shields@jpl.nasa.gov

Abstract— StarLight is a NASA\JPL sponsored mission that will demonstrate formation flying and interferometric technologies needed for future missions such as Terrestrial Planet Finder (TPF). The StarLight stellar interferometer is composed of two spacecraft, a combiner spacecraft and a collector spacecraft, forming separated apertures.

In this paper, the metrology pointing sensor of the StarLight ground instrument prototype is characterized and a siderostat pointing control loop is closed between two optical benches with a 10 meter separation. The Formation Interferometer Testbed (FIT) metrology pointing sensor (MPS) uses four photodiodes to detect gradients in the metrology laser caused by relative motion of the two optical benches. By differencing across the photodiodes, a measurement of the laser beam centroid can be obtained. In the flight design, this signal is passed to the combiner spacecraft, via an interspacecraft communication link, and used as a feedback signal to point a siderostat on the combiner spacecraft.

In this paper, a detailed model of the metrology pointing sensor is described based exclusively on experimental data. Both the sensitivity and dynamic range of the sensor are effectively described by this model. The effect of diffraction in the laser light and air path noise on the sensor performance are evaluated.

A nonlinear estimation algorithm is proposed that is capable of increasing the capture zone of the sensor by a factor of two. This algorithm relies on using the photodiode sum as an additional measurement.

The second part of this paper describes a siderostat pointing control algorithm that uses tachometer, encoder, and the metrology pointing sensor as feedback signals in a nested loop architecture. Experimental results are included that demonstrate the tracking ability of this controller in the presence of spacecraft relative motion caused by Attitude Control System (ACS) deadbands.

TABLE OF CONTENTS

0-7803-7231-X/01/ 10.00 ©2002 IEEE

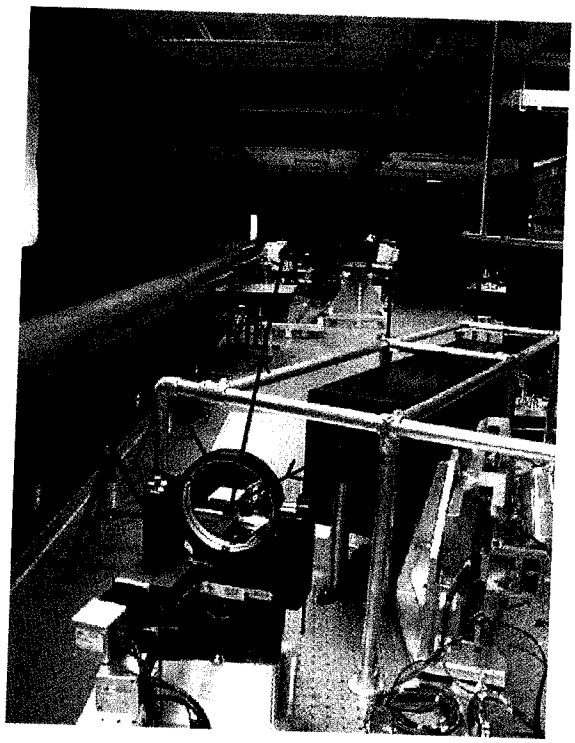

Figure 1. Photograph of the left side of the FIT instrument. The path of the interspacecraft metrology beam is denoted with annotated lines. In the foreground is the left siderostat. The metrology pointing sensor (IGD) is in the background mounted on the collector bench.

1. INTRODUCTION

The FIT interferometer is a ground based prototype of the two spacecraft StarLight instrument. StarLight is a NASA/JPL sponsored technology development mission that will demonstrate formation flying of two spacecraft and interferometric stellar observations [1]. Both space-

craft are used to collect light from separated apertures which is then combined to produced interference fringes on the combiner spacecraft. The interspacecraft metrology pointing system is used to maintain an optical link between the two spacecraft and thereby keep the boresights of the metrology and starlight co-aligned. Maintaining the metrology lock is also necessary to ensure a return signal for the interspacecraft metrology gauge that is used to estimate the fringe position. Furthermore, information from the metrology pointing system, in the form of range and bearing measurements, can be used by the formation estimator to calibrate the autonomous formation flying (AFF) sensors.

The pointing system is composed of a large aperture siderostat on the left side of the combiner spacecraft and a pointing sensor on the collector spacecraft. The pointing sensor is a JPL design developed specifically for the StarLight mission [2]. It is an array of four photodiodes (See Figure 2.) that are selectively sensitive to the wavelength of the metrology laser. By differencing across the photodiodes, measurements of the laser beam position can be derived which are then transferred across a communication link to the combiner spacecraft and used as feedback signals to point the left combiner siderostat.

The metrology pointing sensor assumes that the metrology beam has a Gaussian distribution of intensity and operates by detecting gradients in the photodiode voltages caused by translation of the beam across the face of the sensor. The measurement equations for the sensor are,

$$V_{nx'} = \frac{(V_{igd3} + V_{igd1}) - (V_{igd4} + V_{igd2})}{(V_{igd1} + V_{igd2} + V_{igd3} + V_{igd4} + V_{bias})} \quad (1)$$

$$V_{ny'} = \frac{(V_{igd4} + V_{igd3}) - (V_{igd2} + V_{igd1})}{(V_{igd1} + V_{igd2} + V_{igd3} + V_{igd4} + V_{bias})} \quad (2)$$

where $V_{(\cdot)}$ are the photodiode voltages and V_{bias} is a constant ($V_{bias} = -1$) that is used to keep the measurements well defined when the beam is far from the sensor. Note that $V_{nx'}$ is a measurement of the beam location in the x' direction and $V_{ny'}$ is a measurement of the beam location in the y' direction (Refer to Figure 2 for coordinate frame definitions.).

The FIT testbed is comprised of three main optical benches. The main bench is the combiner bench which collects light on the right side of the instrument from the pseudostar bench and on the left side of the instrument from the collector bench. The collector bench is mounted on a 6 DOF hexapod which allows simulation of spacecraft relative motion, caused in flight, by thruster ACS deadbands. A photo of the left side of the instrument is shown in Figure 1. Note the tube to the left of the photo that can be installed along the path of the metrology beam to reduce the effect of air turbulence.

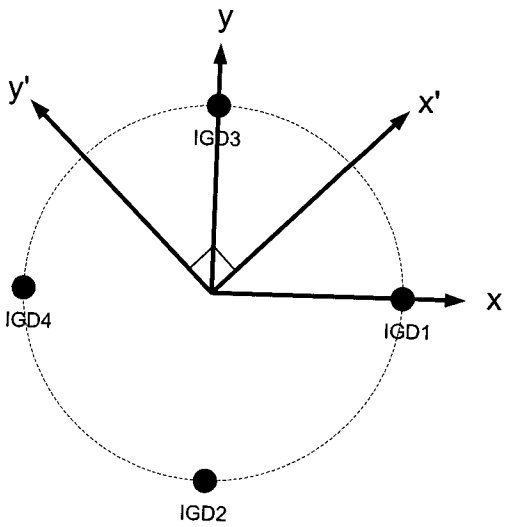

Figure 2. Intensity gradient detector (IGD) photodiode arrangement and coordinate frames. The primed frame is referred to as the sensor frame and the unprimed frame is referred to as the vertical frame.

The siderostat (Aerotech, AOM130-6M) used for metrology pointing has local feedback of both position and velocity provided by encoders mounted on the shafts of two DC motors (BM75E). The amplifiers (BAL 20-40-A) were configured in velocity mode to reduce the effect of friction. The position loop has a closed loop bandwidth of approximately 40 Hertz in both azimuth and elevation axes.

2. System Characterization

Backlash Investigation

The fundamental limitation on the pointing accuracy of the Aerotech siderostats is backlash in the drive mechanism. The Aerotech siderostats are equipped with a 1000 line encoder which, with 4X quadrature and a gear ratio of 25816.7:1, provide a knowledge resolution of up to 12.5 milli-arc seconds at the gimbals. This accuracy cannot be achieved, however, because of backlash in the gimbal drive mechanism.

To determine the actual pointing accuracy, the gimbal position was directly measured using laser metrology. A silicon based light sensitive position sensing device (OnTrak PSM with OT-301 amplifier) with a calibrated scale factor of 2.0e-4 m/volt was used in conjunction with a He-Ne laser source reflected off the mirror to measure the true position of the siderostat gimbal. The PSM was placed 1.16 meters from the mirror with the reflected laser beam impacting the silicon die. An open loop velocity command (either sine or triangle wave) was applied to a given axis while data was recorded from both the encoder and PSM. Results for the azimuth axis are shown in Figure 3. The backlash is clearly detected as the separation of the two lines in this figure. At

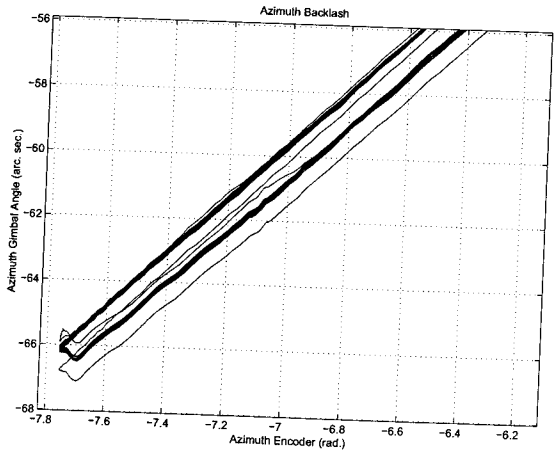

Figure 3. Backlash of the siderostat azimuth axis. Measurements from both the azimuth encoder (x-axis) and angular metrology (y-axis) were used to discern the effect of backlash.

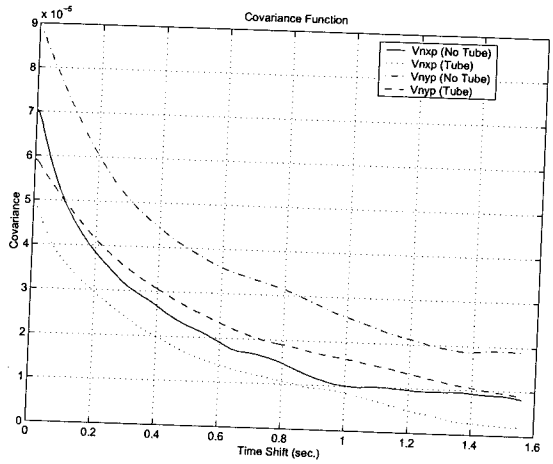

Figure 4. Auto-covariance function of sampled IGD signals with and without a tube installed along the exposed air path.

the azimuth encoder the backlash is approximately 0.175 radians. This represents 1.4 arc seconds of backlash at the azimuth gimbal, much greater than the encoder resolution would predict. The elevation axis was found to have about 0.39 arc seconds of backlash at the gimbal. In both cases the amount of backlash was found to be highly dependent on position.

As to the exact source of the backlash, some simple calculations reveal that the likely culprit is a threaded rod in the Aerotech mounts. The Aerotech drive mechanism is a three stage device. The first stage consists of two sets of spur gears each with a gear ratio of 5:1, for an effective gear ratio, GR_{spur}, of 25:1. The output shaft of the gear box drives a threaded rod with a pitch, p, of 0.113 mm/radian. A universal joint then connects a nut driven by the threaded rod to a lever arm, r, of length 0.115 meters which acts to move the gimbal axis. The overall gear ratio of the three stages is,

$$GR = GR_{spur} \cdot \frac{1}{p} \cdot r. \qquad (3)$$

The first spur gear has 20 teeth which means that for the azimuth axis, there would have to be 0.5 teeth of backlash at this point to explain the amount of backlash seen in this axis. The second contact point in the spur gear box would require 0.1 teeth of backlash. In either case, it is unlikely that there is this much backlash in the gear box, so the source of the backlash is likely after the gear box. The amount of play at the threaded rod to explain 1.4 arc seconds of backlash at the gimbal is only 0.78 microns, or one 886.1th of a thread. This is much more likely the source of the backlash. If the backlash is at this level, preloading the gimbal should help reduce the backlash which was, in fact, found to be the case.

Air Path Disturbance Modelling

In the FIT laboratory the metrology beam is deflected from its nominal path by air currents in the lab. On the left side of the interferometer, this error is sensed at the transfer flat on the collector bench by the IGD sensor, and can be rejected by moving the left combiner siderostat in an appropriate manner. In flight, this feedback loop acts to take out any attitude and translational deadbands caused by the spacecraft ACS. In the FIT lab these deadbands are simulated by moving the collector hexapod. Thus, in the laboratory, the IGD loop has the duel job of taking out the relatively low frequency interspacecraft motion and, if possible, reject the pointing error caused by the higher frequency air path disturbance.

The air path disturbance is by its nature stochastic, but observations of the photodiode voltages (sampled at 256 Hz) reveal that it is correlated in time. Figure 4 reveals that the air path process has a correlation time of approximately 0.3 seconds. This figure is a plot of the auto-covariance function,

$$X_{xx}(\tau) = E\left[(x(\tau) - m_x)(x(t-\tau) - m_x)\right], \qquad (4)$$

where $E[\cdot]$ is the expectation operator, and m_x is the mean value of the signal $x(t)$, for the normalized IGD measureables, $V_{nx'}$ and $V_{ny'}$, with and without the tube installed between the optical benches. Note that with the tube, the variance at all time shifts, τ, is smaller than without the tube. Thus, the tube is somewhat effective at reducing the effect of air turbulence on the beam path. This is what one would expect since the volume of air that the metrology beam passes through is contained and isolated from the external environment when the tube is present. The square root of the peak value of the curves in Figure 4 represents the standard deviation of the air path disturbance. The noise equivalent angle (NEA) at the siderostat gimbal due to the

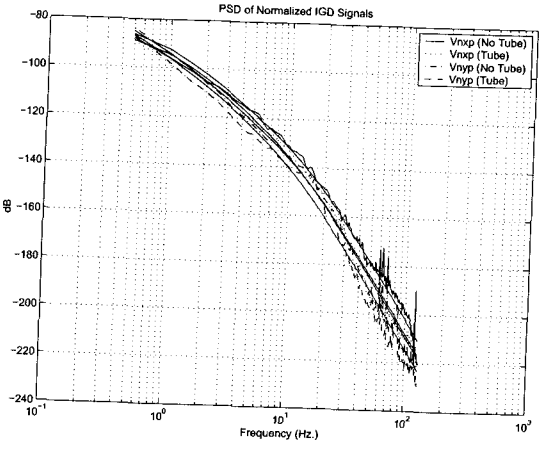

Figure 5. PSD of normalized IGD signals with and without a protective tube installed to mitigate the air path turbulence. Solid lines represent a parametric fit of the frequency domain data.

effect of air path is,

$$NEA_{V_{nx'}} = \frac{2\sigma_{V_{nx'}} SG^{-1}_{V_{nx'}}}{2R} = \pm 1.056\ (arc\,seconds),$$
$$NEA_{V_{ny'}} = \frac{2\sigma_{V_{ny'}} SG^{-1}_{V_{ny'}}}{2R} = \pm 1.159\ (arc\,seconds) \tag{5}$$

where R (10.26 meters) is the distance between the left combiner siderostat and the collector IGD sensor and $SG_{(\cdot)}$ is the scale factor between $V_{n(\cdot)}$ and the displacement of the beam centroid in the IGD coordinate frame. $SG_{V_{nx'}}$ and $SG_{V_{ny'}}$ were calculated by commanding the left combiner siderostat in azimuth and elevation a known amount, and recording the resulting $V_{nx'}$ and $V_{ny'}$ values. A linear fit to this data gave $SG_{V_{nx'}} = 160.86$ 1/meters and $SG_{V_{ny'}} = 163.64$ 1/meters.

For the FIT interferometer ~ 1.0 arc seconds of beam jitter at the left siderostat gimbal represents about 50 microns of shear between the metrology and stellar beams at the IGD transfer flat. This small amount of shear is not large enough to cause any alignment problems in the combiner optics with either the incoming stellar light or return metrology signal.

In order to simulate the effect of the air path turbulence on the pointing control loops, a shaping filter can be designed to match the spectral content of the air path disturbance. The PSD of the sampled time series for $V_{nx'}(t)$ and $V_{ny'}(t)$ is shown in Figure 5. The slope in this plot is -80 dB/decade which indicates that a second order transfer function is needed to model the spectral content of the sampled data. Assuming a two pole model of the form,

$$H(s) = \frac{k}{s^2 + as + b}, \tag{6}$$

where we take as the input, zero mean Gaussian white noise, $w(t)$, with auto-covariance function,

$$E\left[w(t)w(t-\tau)\right] = Q\delta(\tau), \quad (Q = 1) \tag{7}$$

we can parameterize $|H(j\omega)|^2$ in the following linear form,

$$\underbrace{\psi(\omega)\omega^4}_{\mathbf{Y}} = \underbrace{\begin{bmatrix} -\psi(\omega)\omega^2 & -\psi(\omega) & 1 \end{bmatrix}}_{\mathbf{A}} \underbrace{\begin{bmatrix} a^2 - 2b \\ b^2 \\ k^2 \end{bmatrix}}_{\Theta}, \tag{8}$$

where $\psi(\omega)$ is the spectral power, $|H(j\omega)|^2$, at a given frequency, ω. To solve for the transfer function parameters, Θ, this equation can be inverted using a frequency weighted least squares calculation,

$$\Theta = (\mathbf{A^T W A})^{-1}\mathbf{A^T W Y}, \tag{9}$$

where $\mathbf{W}$ is the weighting matrix (diagonal), $\mathbf{Y} \in \Re^{\mathbf{n\times 1}}$ is the vector of left hand values of Equation (8) at n frequency points, and $\mathbf{A} \in \Re^{\mathbf{n\times 3}}$ is the matrix of regressor vectors. This calculation results in the following shaping filters for the case of no tube in the beam path.

$$V_{nx'}(s) = \frac{3.5}{s^2 + 98.1s + 409.1} w_{V_{nx'}}(s)$$
$$V_{ny'}(s) = \frac{2.5}{s^2 + 85.8s + 211.6} w_{V_{nx'}}(s) \tag{10}$$

For implementation in the pointing simulation testbed, these filters were converted to a state space realization and discretized using a first order approximation of the state transition matrix.

$$\dot{\mathbf{x}}(t) = \mathbf{A}\mathbf{x}(t) + \mathbf{B}w(t), \quad V = \mathbf{C}\mathbf{x}(t) \quad \Rightarrow$$
$$\mathbf{x}((k+1)\Delta t) = \mathbf{A}_d\mathbf{x}(k\Delta t) + \mathbf{B}_d\mathbf{w}_d(k\Delta t),$$
$$V_{n(\cdot)}(k\Delta t) = \mathbf{C}\mathbf{x}(k\Delta t) \tag{11}$$

The matrices $\mathbf{A}_d$ and $\mathbf{B}_d$ are defined based on the solution of the continuous time system at discrete time intervals.

$$\mathbf{A}_d = \exp(\mathbf{A}\Delta t) \tag{12}$$
$$\mathbf{B}_d\mathbf{B}_d^T = \mathbf{\Gamma} \tag{13}$$
$$\mathbf{\Gamma} = \exp(\mathbf{A}\Delta t)[\mathbf{B}Q\mathbf{B}^T\Delta t - \frac{1}{2}\Delta t^2\mathbf{B}Q\mathbf{B}^T\mathbf{A}^T$$
$$-\frac{1}{2}\Delta t^2\mathbf{A}\mathbf{B}Q\mathbf{B}^T + \frac{1}{3}\Delta t^3\mathbf{A}\mathbf{B}Q\mathbf{B}^T\mathbf{A}^T](\exp(\mathbf{A}\Delta t))^T \tag{14}$$

The factorization of $\mathbf{B}_d$ in Equation (13) is performed using a Cholesky decomposition. Note that even though the continuous time system has a scalar random input, the equivalent discrete time system has a vector random input with auto-covariance function,

$$E\left[\mathbf{w}_d(k)\mathbf{w}_d(j)\right] = \mathbf{\Gamma}\delta_{kj}. \tag{15}$$

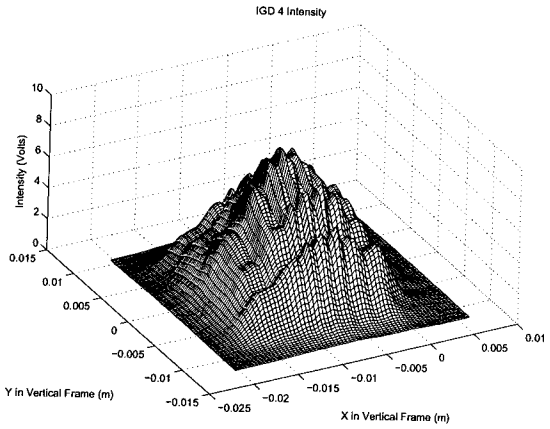

Figure 6. Output voltage of the 4th photodiode as a function of metrology beam location. Note diffraction ripples in both directions caused by the square aperture of the metrology spider.

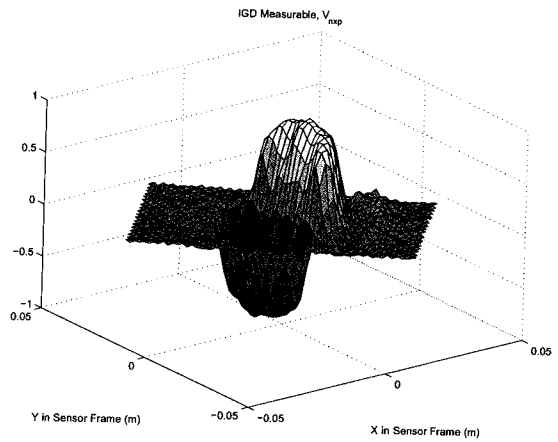

Figure 7. Plot of $V_{nx'}$ as a function of beam position. Note irregularities in the surface along the cross axis.

In characterizing the air path disturbance we have assumed that the random variations in the sampled IGD voltages are due to air currents and not vibrations of the optical bench. If vibrations were responsible for the variations observed from the IGD signals, one would expect that the 4 IGD voltages would be highly correlated in time with one another. This was found not to be the case, however, as the largest correlation coefficient was found to be 0.56, which means only $\sim$ 25 percent of the data in a scatter (x-y) plot between any two of the IGD voltages can be explained using a linear relationship . In either case, the source of the variations are of secondary interest as the control loops will act to reject these disturbances regardless of their source.

Another finding on the effect of air path turbulence in the FIT laboratory is that the amount of pointing error caused by the air path disturbances does not depend on distance. This is perhaps counter to what one might initially think. This effect was observed during the backlash investigation by placing the PSM at different distances from the siderostat mirror. The motivation for doing this was to see which placement gave the best resolution of gimbal angle. For the three distances, 210 mm, 1700 mm, and 10000 mm that were tried, the amplitude of the air path disturbance calculated by,

$$Beam\ Error = \frac{V_{p-p} \cdot 0.2\,(mm/volt)}{range}, \qquad (16)$$

where V_{p-p} is the quiescent (i.e. no siderostat motion) peak to peak variation in PSM voltage, was found to be approximately 1.0 arc seconds for all three placements of the sensor. This implies that the air turbulence causes V_{p-p} to scale linearly with range.

Sensor Characterization

The previous section characterized the stochastic behavior of the IGD signals. What remains, is to determine the bias in each of the IGD signals as a function of the beam displacement. We already have a coarse model for the bias from calculating $SG_{V_{nx'}}$ and $SG_{V_{ny'}}$ in Equations (5). A more accurate model of the static IGD output was obtained by scanning the metrology beam across the face of the transfer flat and sampling the four IGD signals. The scanning was sinusoidal in the azimuth direction and ramped downward in the elevation direction from a position slightly above the IGD sensor. Figure 6 shows the result of this experiment for the 4th IGD photodiode. This figure is essentially a photograph of the metrology beam intensity. To model the IGD sensor in the simulation testbed, look up tables containing the data shown in Figure 6, for each of the four photodiodes were used.

Note the diffraction pattern that is superimposed on Figure 6. This pattern is caused by obscuration of the metrology beam as it exits the square aperture of a metrology spider located on the combiner bench. The effect of these ripples, together with possibly too large of a photodiode radius relative to the beam diameter, is to introduce a large amount of uncertainty in the relationship between the IGD measurables, Equations (1)-(2), and beam location. Knowledge of this relationship becomes important during design of the metrology pointing control algorithm. In addition, if an estimator (i.e. Kalman Filter) is used to estimate the impact position of the metrology beam based on IGD measurements, this uncertainty could cause either local minimum in the optimization algorithm or large estimation errors due to the modelling error introduced by the smoothing of the surfaces that would be necessary to avoid the local minimum. These effects were observed using an estimator design based on Fourier transforms to model the surface functions $V_{nx'} = V_{nx'}(x', y')$ and $V_{ny'} = V_{ny'}(x', y')$.

Figure 7 is a plot of $V_{nx'}(x', y')$. Note in this figure that the IGD measurable, $V_{nx'}$, is not a single valued function. The measurement is linear within a certain distance ($\sim \pm 6.0$ mm) of the photodiode array center, beyond which it de-

creases back to zero as the beam no longer exposes any of the photodiodes. As a result, the capture range of the sensor is restricted to be within the linear range, since otherwise it would not be possible to discern, from a given measurement, whether or not the beam was inside or outside of the linear range. To overcome this limitation, measurements (1) and (2) can be augmented with the sum measureable,

$$V_\Sigma = V_{igd1} + V_{igd2} + V_{igd3} + V_{igd4}. \quad (17)$$

The sum information is enough to clarify the beam position ambiguity. If the sum is large, then the beam is within the linear region, else if the sum is small then the beam is outside the linear region. An estimator of the beam position would then use measurements in the form of,

$$\begin{bmatrix} V_{nx'} \\ V_{ny'} \\ V_\Sigma \end{bmatrix} = \mathbf{h}(x', y'), \quad (18)$$

where $\mathbf{h}(x', y')$ is a highly nonlinear vector function. Theoretically, with noiseless measurements, this approach offers the possibility of making the capture range of the sensor infinite. Practically, however, we should expect a 2X increase in the capture range. This idea is not pursued further in this paper as it would require a significant divergence from the intended topics of the paper.

3. Acquisition

The acquisition of the metrology signal is a critical step in the observation sequence of the instrument. It represents the first optical link between the two spacecraft and is a prerequisite for acquisition of the left side starlight. To acquire feedback signals from the IGD sensor for the metrology loop, a spiral search is performed. The search is designed to be optimal within the constraint that the velocity limits on the siderostat are never exceeded. To achieve this, we parameterize the search in polar coordinates with,

$$\begin{aligned} r &= \frac{g}{2\pi}\theta \\ \theta &= f(t), \end{aligned} \quad (19)$$

where r and θ are the polar coordinates of a cartesian frame located at the center of the IGD sensor. g is the spacing between adjacent spirals, which should be configured to be less then the dynamic range of the IGD sensor. $f(t)$ is some, as yet, undetermined function of time. This function can be specified by observing that if the local velocity along the pathlength of the spiral is constant, the velocity commands to the siderostat axes will be sinusoids with a constant amplitude. This amplitude can be adjusted to be slightly less than the siderostat velocity limit by specifying the pathlength velocity. In cartesian coordinates the pathlength velocity is given by,

$$s = \sqrt{\dot{x}^2 + \dot{y}^2}, \quad (20)$$

where,

$$\begin{aligned} x &= r\cos(\theta) \\ y &= r\sin(\theta). \end{aligned} \quad (21)$$

Substituting Equations (21) and (19) into (20), we arrive at the following differential equation,

$$\dot{f}(t) = \pm\sqrt{\frac{(2\pi s/g)^2}{1 + f(t)^2}} \qquad f(0) = 0, \quad (22)$$

which describes the time evolution of $\theta(t)$ for the optimal spiral search. This equation was solved numerically, in real time, for trajectory generation of the acquisition spiral. The $(+)$ solution is used for outward spirals and the $(-)$ solution is used for inward spirals. The siderostat encoder commands are obtained from,

$$\begin{aligned} \theta_{El.} &= -\left(\frac{y}{2d}\right) \cdot GR \\ \theta_{Azi.} &= -\left(\frac{x}{2d}\right) \cdot GR, \end{aligned} \quad (23)$$

where x and y come from Equation (21) and d is the separation between the spacecraft.

Although we have formulated the problem with respect to constraints on the siderostat velocity, the solution is also applicable to situations which have a velocity constraint on the spiral imposed by the sensor's ability to detect changing signals.

4. Controller Design

A model of the pointing system is shown in Figure 8. This model includes three effects on the beam position sensed by the IGD sensor. First, is the effect from moving the siderostats, which is the controlled variable in the system. Second, is the stochastic air path disturbance. Third is the hexapod motion which is modelled as a ramp position disturbance. Even though the actual interaction of the 6 DOF hexapod motion with the IGD sensor is much more complicated, this model should be adequate for the small translations and rotations of the hexapod that simulate thruster deadbands.

Note that because the siderostat azimuth and elevation axes control the beam position in vertical frame, and the measurements are made in the sensor frame, the sensor and actuator are coupled by the rotation matrix, $\mathbf{R}_z^T$. The matrix $\mathbf{K}$ in Figure 8 represents the interspacecraft kinematics, which for the flight system would include the effects of spacecraft attitudes and relative position. For the FIT lab, this matrix was taken to be simply,

$$\mathbf{K} = \begin{bmatrix} -2 \cdot R & 0 \\ 0 & -2 \cdot R \end{bmatrix}. \quad (24)$$

Looking a Figure 8, the controller first acts to invert the input\output relationship of the IGD sensor using a linear approximation,

$$SG^{-1} = \begin{bmatrix} SG_{V_{nx'}} & 0 \\ 0 & SG_{V_{ny'}} \end{bmatrix}^{-1}. \quad (25)$$

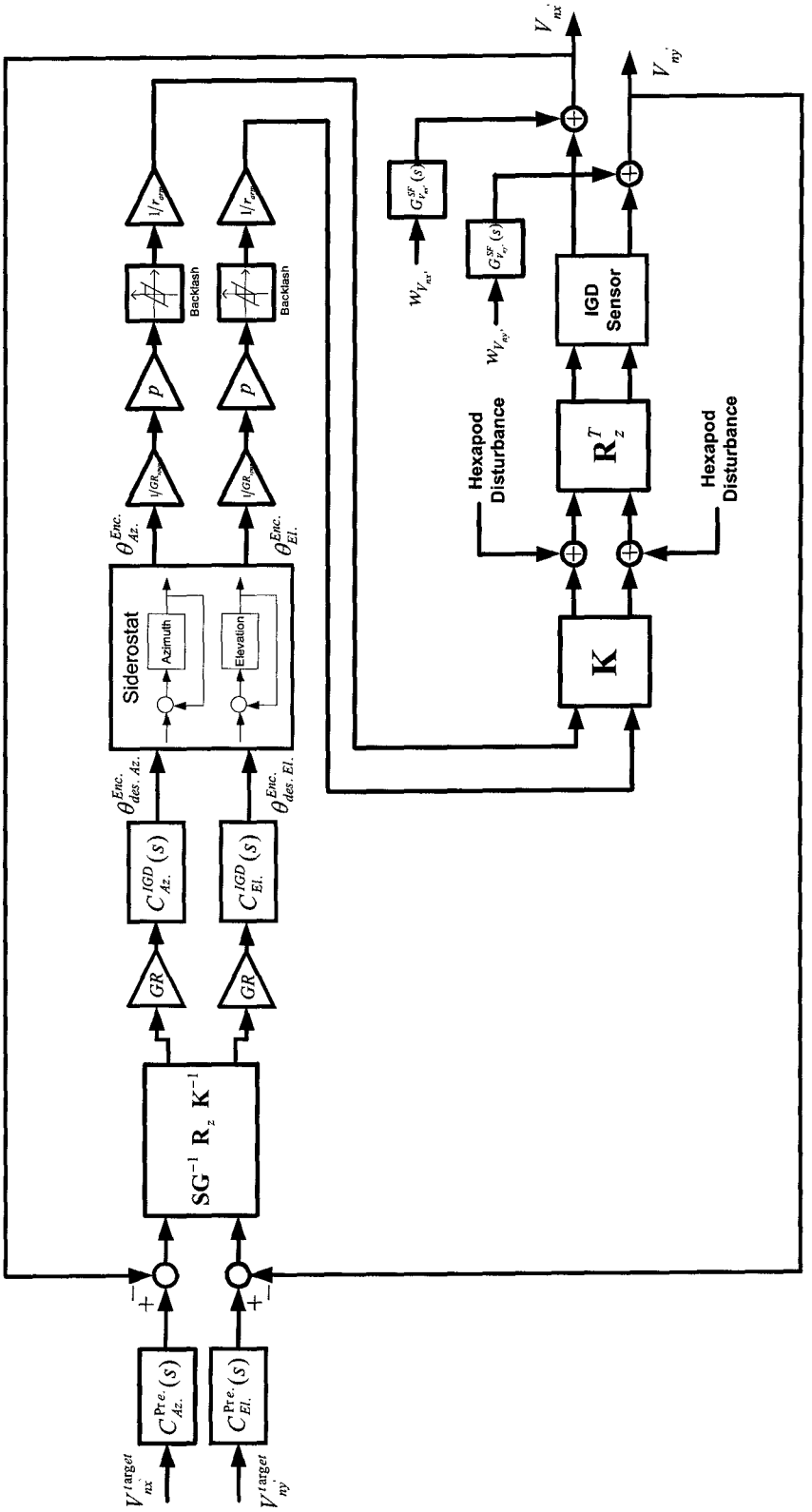

Figure 8. Model of IGD pointing system and control algorithm. The effect of hexapod motion, air path turbulence, and backlash are included in the pointing model. The controller diagonalizes the system and controls each axis as though they were SISO loops.

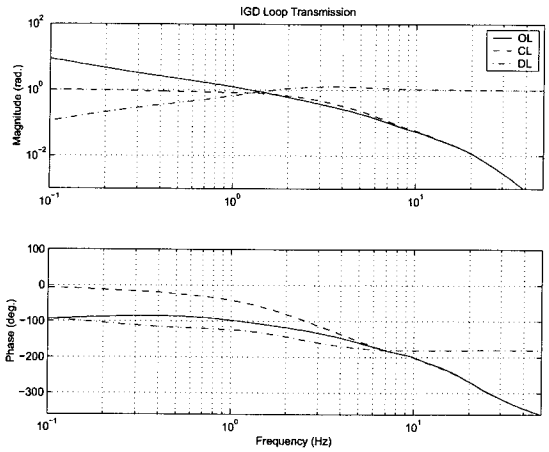

Figure 9. Open loop, closed loop, and disturbance attenuation of the metrology pointing system.

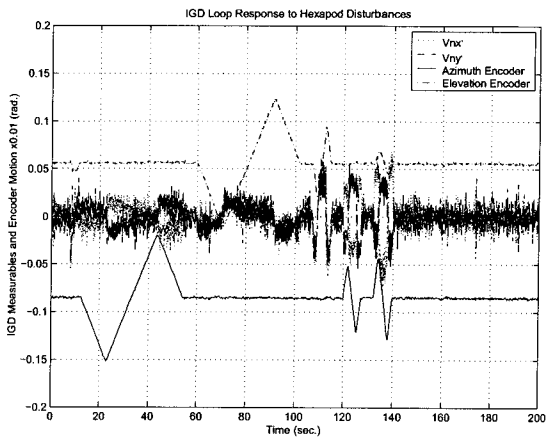

Figure 10. Experimental response of the metrology pointing system to disturbances introduced by hexapod motion.

The pointing system is then diagonalized by inverting the coupling between the sensor frame and siderostat gimbals. The error signal is then mapped to encoder space with the $\mathbf{K}^{-1}$ and GR control gains. With the system decoupled the dynamic part of the compensator can now be designed as if there were no coupling [3]. This is advantageous since SISO (Single Input Single Output) design can be less conservative then MIMO (Multiple Input Multiple Output) design. The azimuth and elevation loop shapes can be designed separately by treating,

$$C_{Az}^{IGD}(s)G_{Az}^{SD}(s) \tag{26}$$

$$C_{El}^{IGD}(s)G_{El}^{SD}(s) \tag{27}$$

as the effective open loop transfer functions. $G_{Az}^{SD}(s)$ and $G_{El}^{SD}(s)$ in these equations are the closed loop transfer functions from desired encoder position to actual encoder position.

Loop Shaping

To reject the air path disturbance the open loop control system must have a crossover well above the poles of the disturbance process. This ensures that the sensitivity of the control error to air path disturbances,

$$S(s) = \frac{-1}{1 + C_{(\cdot)}^{IGD}(s)G_{(\cdot)}^{SD}(s)}, \tag{28}$$

is small at frequencies where the disturbance is large. To achieve significant disturbance attenuation the compensator would have to be designed to provided an open loop bandwidth of approximately 50.0 Hz. Simulations of a system with this bandwidth displayed oscillatory behavior. The likely source of the instability was phase lag induced by the siderostat backlash [4]. It was empirically determined that the maximum bandwidth achievable in the laboratory was approximately 2.0 Hz (See Figure 9.). With this bandwidth, achieving any significant atmospheric rejection was not possible and the goal of the IGD control loop was limited to taking out the lower frequency hexapod motions.

Spacecraft thruster deadbands introduce "ramp" type disturbances into the metrology pointing system. In order to have zero steady state error with this type of disturbance, the compensator is required to have two integrators. Two phase lead components and a notch filter were added to achieve a graceful degradation of the phase in the crossover region. The overall compensator was 6th order. A prefilter was added to the input channels to avoid saturation from step changes in the target IGD measurables. Note that commands are given to the pointing loop in terms of desired $V_{nx'}$ and $V_{ny'}$ values. This is convenient in that commands between ± 1.0 are guaranteed to be within the capture range of the sensor.

Experimental Results

The response of the control system is shown in Figure 10. The hexapod was commanded to move in both translation and rotation. The translational motion was in a plane perpendicular to the metrology beam, first in the horizontal direction and second in the vertical direction, both at a rate of 0.5 mm/second., twice the "observation" mode control requirement for a 40 meter baseline [5]. The rotational motion was along each of the axes of the hexapod coordinate frame by an amount of ± 0.5 degrees.

Note that as the hexapod is slewed in the horizontal direction, the siderostat azimuth axis moves to track the location of the IGD. When the hexapod is slewed in the vertical direction, the elevation axis responds to track the IGD. In either case, the IGD signals asymptotically approach zero confirming proper operation of the control system. The second half of Figure 10 shows the response of the control system to rotational motion of the hexapod. The control errors are larger in this case, but the rotation rate was well above the attitude rate control specification [5].

5. Conclusions

This paper has presented a pointing model and control algorithm for the FIT angular metrology system. Performance of the system was demonstrated to be sufficient to cancel the effects of the spacecraft relative motion. For flight, it is anticipated that the basic structure of the algorithm could remain relatively unchanged. Modifications for varying baselines and changing relative attitudes of the two spacecraft should be straightforward. Since the IGD measurements are normalized, the sensor gain should be insensitive to attenuation of the beam intensity for larger spacecraft separations. In flight, a single calibration of the sensor at an intermediate spacecraft separation should be adequate for control purposes.

The backlash in the Aerotech siderostats was found to limit both the pointing accuracy and bandwidth of the control system. It should be mentioned that similar backlash numbers for this Aerotech model have been reported from the Keck interferometer. A direct drive gimbal would be more appropriate for interferometry applications.

6. Acknowledgments

The authors would like to thank Gary Blackwood for his support of this research. The work described in this paper was carried out at the Jet Propulsion Laboratory, California Institute of Technology, under a contract with the National Aeronautics and Space Administration.

References

[1] R. Duren and O. Lay, "The StarLight formation-flying interferometer system architecture," Big Sky, Montana, March 2002, IEEE Aerospace Conference, IEEE.

[2] A. Abramovici, "Intensity gradient detector for FIT: A user's guide," Tech. Rep., Jet Propulsion Laboratory, 2000.

[3] B. J. Lurie and P. J. Enright, *Classical Feedback Control With MATLAB*, Marcel Dekker Inc., New York, 2000.

[4] J. J. E. Slotine and W. Li, *Applied Nonlinear Control*, Prentice-Hall, 1991.

[5] A. Ahmed, "Starlight FACS requirements," 2001.

[6] M. Born and E. Wolf, *Principles of Optics*, Cambridge University Press, 1999.

[7] B. J. Lurie, J. J. Hench, A. Ahmed, and F. Y. Hadaegh, "Nonlinear control of the optical delay line pathlength," Orlando, Florida, April 1999, SPIE, vol. 3692, pp. 139–149.

[8] J. Shields, S. Sirlin, and M. Wette, "Starlight pointing subsystem for the formation interferometer testbed (FIT)," Big Sky, Montana, March 2002, IEEE Aerospace Conference, IEEE.

[9] R. K. Tyson, *Principles of Adaptive Optics*, Academic Press, 1991.

[10] J. W. Goodman, *Introduction to Fourier Optics*, McGraw-Hill, 1968.

[11] S. Dubovitsky, O. Lay, and A. Abramovici, "The StarLight metrology subsystem," Big Sky, Montana, March 2002, IEEE Aerospace Conference, IEEE.

Joel Shields *is a member of the Guidance and Control Analysis Group at the Jet Propulsion Laboratory. He received his B.S. degree in Applied Mechanics from U.C. San Diego in 1990 and his M.S. and Ph.D. degree in Control Systems from U.C. Berkeley in 1993 and 1997, respectively. His dissertation research was on control of exercise machines. He is the holder of a patent based on this work. Upon graduation, Dr. Shields worked as a consultant before joining the technical staff at JPL. Dr. Shields has extensive experience in design of mechatronic systems, system identification, adaptive control, precision servo control, and real time applications of control systems. Currently, he is working on pointing control for space based interferometry.*

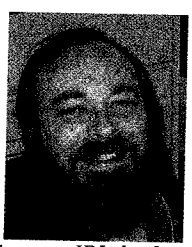

Samuel Sirlin *has a Ph.D. in Mechanical Engineering from Columbia University (1983). From October 1983 to the present he has been a member of the Technical Staff at JPL. His background and expertise covers the areas of dynamics and simulation, controls and estimation. During his time at JPL he has worked on a number of research and flight projects including Galileo, Ulysses, Mars Pathfinder, Deep Space 1 (DS1), Starlight, Mars Exploratory Rover (MER), Control Structure Interaction research, Modelling and Analysis for Controlled Optical Systems (MACOS), and Integrated Modelling of Optical Systems (IMOS). He has published 26 conference papers and 4 journal articles.*

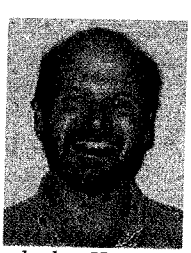

Matt Wette *is a Senior Engineer at the Jet Propulsion Laboratory in the Guidance and Control Analysis Group. His interests are in control system design, real-time systems, and discrete event control. Dr. Wette has contributed to several projects in the development of real-time simulation testbeds. He is currently working on interferometer control for the StarLight project.*